https://doi.org/10.5194/egusphere-2025-101
Preprint. Discussion started: 11 April 2025

Measurement report: Formation and brownness of aqueous secondary organic aerosol from the aged biomass-burning emissions in the Sichuan Basin, China

Chao Peng[1,2,3,4], Yan Ding[4], Zhenliang Li[1,2,3], Tianyu Zhai[4], Xinping Yang[4], Mi Tian[6], Yang Chen[5], Xin Long[5], Haohui Tang[6], Guangming Shi[7], Liuyi Zhang[8], Kangyin Zhang[8], Fumo Yang[7], and Chongzhi Zhai[1,2,3]

[1]Chongqing Academy of Ecology and Environmental Sciences, Chongqing, 401336, China

[2]Chongqing Branch Academy of Chinese Research Academy of Environmental Sciences, Chongqing, 401336, China

[3]Chongqing Key Laboratory of Urban Atmospheric Environment Observation and Pollution Prevention, Chongqing, 401336, China

[4]Chinese Research Academy of Environmental Sciences, Beijing 100012, China

[5]Chongqing Institute of Green and Intelligent Technology, Chinese Academy of Sciences, Chongqing, 400714, China

[6]College of Environment and Ecology, Chongqing University, Chongqing, 400045, China

[7]College of Carbon Neutrality Future Technology, Sichuan University, Chengdu, 610065, China

[8]Chongqing Three Gorges University, Wanzhou, 404000, China

Correspondence: Chao Peng (pengchao0623@sina.com) and Chongzhi Zhai (czz66818@sina.com)

https://doi.org/10.5194/egusphere-2025-101
Preprint. Discussion started: 11 April 2025

Abstract. Secondary organic aerosol (SOA) formed via complex chemical mechanisms was the major contributor to atmospheric aerosol pollution and climate forcing worldwide. The aqueous-phase oxidation was an important pathway for SOA formation and the aqueous SOA (aqSOA) exhibited absorption properties across ultraviolet to visible range. Here, we reported the direct ambient observation of SOA formation and absorption properties in the aqueous phase from the Sichuan Basin, China. Considerable aqSOA was originated from the aged biomass-burning emissions via aqueous-phase reactions instead of photo-chemical reactions under high aerosol liquid water content (ALWC) conditions, especially during the polluted period. The substantial impact on brown carbon (BrC) absorption from SOA was observed from 370 nm to 660 nm (27.5%−43.2%). This study highlighted the significant contribution of aqSOA formation from aged biomass-burning emissions to the BrC budget and absorption, especially at night. The mean aerosol absorption Ångström exponents from 370 nm to 880 nm ($AAE_{370–880}$) was 1.95, higher than that observed in fresh and photo-chemically aged biomass-burning emissions. This study revealed the aqSOA formation and brownness from aged biomass-burning emissions and highlighted the importance of aqueous-phase reactions on air quality and climate.

Keywords: Particulate matter; Secondary organic aerosol; Aqueous-phase oxidation; Aged biomass-burning emissions; Brown carbon.

https://doi.org/10.5194/egusphere-2025-101
Preprint. Discussion started: 11 April 2025

1 Introduction

Organic aerosol (OA) was the dominant component (20 to 90%) of atmospheric aerosol with significantly implications for air quality and climate forcing (Jimenez et al., 2009). Numerous field observations indicated that secondary OA (SOA), formed by atmospheric oxidation of volatile organic compounds (VOCs) and primary OA (POA), accounted for most of OA worldwide (Ervens et al., 2011; Huang et al., 2014; Kourtchev et al., 2016). Recent results showed that aqueous-phase oxidation was an important pathway for SOA formation and these SOA production (aqSOA) exhibited absorption properties across ultraviolet (UV) to visible (Vis) range (Gilardoni et al., 2016; Lim et al., 2010; McNeill 2015; Powelson et al., 2014; Sun et al., 2010). However, the formation mechanisms and absorption properties of aqSOA were poorly understood, hindering to improvement of air quality and reducing the uncertainties in global climate estimations.

An increasing number of studies pointed toward aqSOA as a major SOA could form in fogs, clouds, and aerosol water, and oxygenated VOCs (OVOCs) with large water-soluble and low Henry's constant (i.e., methylglyoxal and glycolaldehyde) were the important aqSOA precursors (Ervens et al., 2011; Ortiz-Montalvo et al., 2012; Tan et al., 2012; Xu et al., 2022). A few laboratory studies investigated the levoglucosan and phenolic species produced from biomass burning could also act as aqSOA precursors (Yu et al., 2016; Zhao et al., 2014). Gilardoni et al. (2016) reported direct ambient observations of aqSOA formation from biomass-burning emissions in fog water and wet aerosol. Additionally, recent studies indicated that aqSOA with high

https://doi.org/10.5194/egusphere-2025-101
Preprint. Discussion started: 11 April 2025

molecular weight (i.e., 4-ethylphenol) formed by aqueous-phase photochemical oxidation showed strong light absorptivity within UV range (Herrmann et al., 2015; Ye et al., 2019). Previous laboratory studies also demonstrated that aqSOA, such as π-conjugated compounds and imidazole with C=N bonds produced by aldol condensation and aqueous-phase carbonyl compound reactions respectively, would strongly absorb light at near-UV (Drozd and McNeill, 2014; Kampf et al., 2012; Nozière and Esteve, 2007; Powelson et al., 2014). Despite numerous studies reported on the formation and optical properties of aqSOA, limited research on its ambient observations hindered to better understand the role of aqSOA in atmospheric chemistry and climate.

China experienced severe $PM_{2.5}$ pollution under the stagnant high-humidity conditions, when SOA as the major component was originated from fossil fuel combustion and biomass burning (Huang et al., 2014; Wang et al., 2016; Wang et al., 2021; Xu et al., 2022). Field observations indicated that highly oxidized SOA could form through aqueous-phase processing driven by acid-catalyzed oxidation (Meng et al., 2020; Xu et al., 2017), and considerable aqSOA was formed from biomass-burning OA (BBOA) and fossil-fuel OA via aqueous-phase reactions (Wang et al., 2021; Zhao et al., 2019). A few laboratory studies found aqueous-phase reactions were an important oxidation pathway for nitrophenol products (i.e., 5-nitrovanillin and 4-nitroguaiacol) with strong UV absorption and higher formation and transformation rates were observed in more acidic solutions (Kroflic et al., 2015; Li et al., 2023; Pang et al., 2019; Yang et al., 2021). However, observations on aqSOA

https://doi.org/10.5194/egusphere-2025-101
Preprint. Discussion started: 11 April 2025

formation and optical properties in China were limited and most research concentrated on the North China Plain (NCP). Similar to NCP, the Sichuan Basin (SCB) characterized by high humidity and frequent biomass burning was also the main region with severe aerosol pollution in China (Tian et al., 2019; Wang et al., 2018; Yang et al., 2011). Currently, few studies explored the dynamic evolution and optical properties of aqSOA, and the knowledge of ambient aqSOA processing was still limited in SCB. Therefore, a more detailed characterization of aqSOA formation and optical properties was of great importance to reveal the key factors contributing to haze formation.

Here a time-of-flight aerosol chemical speciation monitor (ToF-ACSM) and a series of collocated instruments were used to characterize aqSOA dynamic evolution from biomass burning under real ambient conditions in a typical city in SCB from October 21 to November 23, 2022. We observed that the haze formation was largely driven by BBOA and aqSOA. We demonstrated considerable aqSOA was originated from the aged BBOA via aqueous-phase reactions. Finally, we further showed that aqSOA produced from aged BBOA were strong UV absorption with positive radiative forcing. These results revealed the aqSOA formation and brownness from aged biomass-burning emissions and helped simulate the associated influences on atmospheric chemistry and climate.

https://doi.org/10.5194/egusphere-2025-101
Preprint. Discussion started: 11 April 2025

2 Methods

2.1 Sampling site

An intensive field campaign on the chemical and physical properties of aerosol was conducted at a site in a severe aerosol pollution city (Yongchuan, 29°21′25″ N, 105°54′6″ E) from October 21 to November 23, 2022. This was a typical urban site located in a parallel ridge-and-valley area between two megacities in SCB (Chongqing center and Chengdu). It was primarily influenced by multiple local emissions from traffic (arterial roads to the east 600 m and west 300 m) and a variety of residential sources (i.e., biomass burning and fossil fuel combustion). Measurements at the site were not interfered by neighboring buildings and helped understand the characteristics of haze pollution dynamic evolution.

2.2 Instrumentation

During the campaign, the non-refractory aerosol (NR-$PM_{2.5}$) species, including organics (Org), ammonium (NH_4), nitrates (NO_3), sulfates (SO_4), and chlorides (Chl), were measured on-line by ToF-ACSM (Aerodyne Research Inc.). Ambient aerosols were pumped into ToF-ACSM at a flow rate of 3 L min^{-1} through a $PM_{2.5}$ cyclone (URG-2000-30ED) and a Nafion dryer (MD-110-48S, Perma Pure, Inc.) reducing the relative humidity to below 30%. The measurement principle was described in detail in the previous studies (Fröhlich et al., 2013; Ng et al., 2011). The ionization efficiency (IE) and relative ionization efficiency (RIEs) were regularly calibrated by a scanning mobility particle sizer with a differential mobility analyzer (SMPS 3081A, TSI) and a

https://doi.org/10.5194/egusphere-2025-101
Preprint. Discussion started: 11 April 2025

condensation particle counter (CPC 3775, TSI). The comprehensive overview of the operation and calibration procedures of ToF-ACSM could be found in Bao et al. (2023).

A seven-wavelength Aethalometer (AE33, Magee Scientific) was used to measure the aerosol light absorption (Abs_λ) and black carbon (BC_λ) mass concentrations in real time at 370, 470, 520, 590, 660, 880, and 950 nm. The sampled particles were dried by a Nafion dryer (MD-70024S-3, Perma Pure, Inc.) before entering into AE33. The light attenuation coefficients were converted to Abs_λ based on the real-time compensation parameter, and the nonlinear loading effects of quartz filters were dealt with on-line by the parallel measurements of attenuation values (ATN1 and ATN2) (Coen et al., 2010; Drinovec et al., 2015). The scattering effects of quartz filters were modified automatically by a fixed multiple scattering parameter (2.14). Detailed measurement methods and principles of AE33 could be found in Drinovec et al. (2015).

During the campaign, the gaseous species (including NO_2 and CO) were continuously measured by gas analyzers (42i and 48i, Thermo Scientific), that were maintained and calibrated weekly. Hourly meteorological parameters data including temperature (T), relative humidity (RH) and $PM_{2.5}$ mass concentrations were obtained on-line from the measurements at the National Environmental Monitoring Station, which was close to our sampling site (http://www.cnemc.cn/).

https://doi.org/10.5194/egusphere-2025-101
Preprint. Discussion started: 11 April 2025

2.3 Data analysis

2.3.1 ToF-ACSM data analysis

The raw mass spectra data measured by ToF-ACSM were analyzed using Tofware v2.5.13 (Tofwerk AG) in Igor Pro 6.37 (WaveMetrics, Inc.). In accordance with previous studies, the default RIEs values for Org, NO_3, and Chl were set to 1.4, 1.1, and 1.3, respectively (Canagaratna et al., 2007; Elser et al., 2016). The IE value (236 ions pg^{-1}) and RIEs of SO_4 (1.2) and NH_4 (4.3) were estimated from the calibrations of pure ammonium nitrate and ammonium sulfate, respectively. The collection efficiency (CE) was set to 0.5 considering the minor influences of low RH dried by Nafion dryer (< 30%), low fraction of ammonium nitrate in NR-$PM_{2.5}$ (31%), and ammonium-rich conditions (Fig. S1) (Matthew et al., 2008; Middlebrook et al., 2012; Zhao et al., 2019). Additionally, the strong correlation between NR-$PM_{2.5}$ and $PM_{2.5}$ mass concentrations supported that the CE value was reasonable (Fig. S2).

The mass spectral matrix of OA for m/z 10−120 was analyzed by positive matrix factorization (PMF) and multilinear engine (ME2) implemented with the SoFi 6.3 (Canonaco et al., 2013; Paatero 1999; Paatero and Tapper 1994). Briefly, unconstrained PMF was used to determine the numbers and types of source factors, then the restriction method ME2 was used to minimize PMF rotational ambiguity by the *a*-values from 0 to 1 with a step of 0.1 (Wang et al., 2019; Zhong et al., 2021). The ions data with signal-to-noise (S/N) lower than 0.2 were discarded, and those S/N from 0.2−2 were downweighted by a factor of 2 (Bao et al., 2023). Finally, five OA factors with function of the rotational parameter (f_{peak} = 0) were identified, including

https://doi.org/10.5194/egusphere-2025-101
Preprint. Discussion started: 11 April 2025

BBOA, coal-combustion OA (CCOA), hydrocarbon-like OA (HOA), oxygenated OA (OOA), and aqSOA. The details of OA source apportionment procedures were described in SI Text S1.

2.3.2 Aerosol liquid water content

During the campaign, the aerosol liquid water content (ALWC) was estimated by the ISORROPIA-II model based on the ammonium, nitrates, sulfates, and chlorides mass concentrations from ToF-ACSM and the meteorological parameters (T and RH) from National Environmental Monitoring Station (Fountoukis and Nenes, 2007). Here, the forward type and metastable mode were used in the ISORROPIA-II model (Hennigan et al., 2015). The thermodynamic equilibrium of the NH_4^+–SO_4^{2-}–NO_3^-–Cl^-–H_2O system was modeled and ALWC was then calculated.

2.3.3 Light absorption measurements

The Abs_λ was divided into BC and brown carbon (BrC, a group of colored OA compounds) absorption ($Abs_{\lambda,BC}$ and $Abs_{\lambda,BrC}$) ($Abs_\lambda = Abs_{\lambda,BC} + Abs_{\lambda,BrC}$) and characterized by the absorption Ångström exponents (AAE) (Laskin et al., 2015). Here, Abs_λ was determined dependent BC_λ mass concentrations ($Abs_\lambda = BC_\lambda \times MAC_\lambda$). We assumed the mass absorption cross-section of aerosols (MAC_λ) were 18.47, 14.54, 13.14, 11.58, 10.35, 7.77, and 7.19 $m^2\ g^{-1}$ at 370, 470, 520, 590, 660, 880, and 950 nm, respectively (Drinovec et al., 2015; Zhu et al., 2017). Here, Abs_{880} was sole from BC and the following formula was used to determine $Abs_{\lambda,BC}$ values: $Abs_{\lambda,BC} = Abs_{880} \times (\lambda/880)^{-AAE_{BC}}$ (Kirchstetter and Novakov, 2004; Moosmüller et al.,

https://doi.org/10.5194/egusphere-2025-101
Preprint. Discussion started: 11 April 2025

2009). The AAE of BC (AAE_{BC}) value was obtained from the equality: $AAE_{BC}=-\log(Abs_{880}/Abs_{950})\div\log(880/950)$ (Wang et al., 2021). Additionally, $Abs_{\lambda,BrC}$ was caused by primary and secondary BrC light absorption ($Abs_{\lambda,BrC,pri}$ and $Abs_{\lambda,BrC,sec}$). The $Abs_{\lambda,BrC,sec}$ value was calculated by a minimum R-squared (MRS) method at each wavelength (Wang et al., 2019; Wu and Yu, 2016; Wu et al., 2024). The detailed information of MRS method and $Abs_{\lambda,BrC,sec}$ estimation was provided in SI Text S2.

The multiple linear regression (MLR) method was used to analyze the light absorption of different OA component at each wavelength: $Abs_{BrC}=a\times[OOA]+b\times[BBOA]+c\times[CCOA]+d\times[aqSOA]+e\times[HOA]$ (Qin et al., 2018; Xie et al., 2019). The [OOA], [BBOA], [CCOA], [aqSOA], and [HOA] indicated the mass concentrations of OA species; the a–e were constants, used to optimize the Abs_{λ} of each OA component, and were equivalent to MAC values at each wavelength. Here, the normalized mean bias (NMB), root mean square error (RMSE), and index of agreement (IOA) were used to evaluate the performance of the MLR method (SI Text S3) (Li et al., 2011). The IOA values of $Abs_{370,BrC}$ and $Abs_{470,BrC}$ (0.99 and 1.00) exceeded 0.95. The slopes of the relationship between $Abs_{370,BrC}$ and $Abs_{470,BrC}$ measured by AE33 and estimated by MLR method were 0.81 and 0.96 (close to unity), respectively. These results indicated a good agreement of $Abs_{370,BrC}$ between AE33 measurement and the MLR reconstruction.

https://doi.org/10.5194/egusphere-2025-101
Preprint. Discussion started: 11 April 2025

3 Results and discussion

3.1 General descriptions

The temporal variations of $PM_{2.5}$ species concentrations, meteorological parameters, $Abs_{370,BrC}$ and $MAC_{370,BrC}$ during the campaign were shown in Fig. 1. The winds were weak with 0.3 ± 0.2 m s^{-1} over the whole campaign, indicating the atmosphere was in stagnant conditions. The total $PM_{2.5}$ (BC+NR-$PM_{2.5}$) mass concentration ranged from 7.0 to 175.5 μg m^{-3}, with an average of 48.4 ± 27.8 μg m^{-3} during the campaign. The average concentrations of Org, NO_3, SO_4, NH_4, Chl, and BC were 24.1 ± 18.1, 8.3 ± 6.2, 6.2 ± 3.4, 5.2 ± 2.7, 0.2 ± 0.1, and 4.7 ± 2.9 μg m^{-3}, taking up 46.6 ± 10.7%, 17.7 ± 8.0%, 13.2 ± 4.4%, 11.2 ± 2.7%, 0.3 ± 0.2%, and 10.1 ± 5.5% of total $PM_{2.5}$, respectively. Org constituted the largest fraction of total $PM_{2.5}$, highlighting the importance of OA in $PM_{2.5}$ pollution in SCB (Bao et al., 2023; Wang et al., 2018). Meanwhile, the high values of $Abs_{370,BrC}$ and $MAC_{370,BrC}$, ranging from 5.8 to 210.2 Mm^{-1} (42.4 ± 28.5 Mm^{-1}) and from 0.6 to 7.0 m^2 g^{-1} (2.1 ± 0.9 m^2 g^{-1}) respectively, were observed during the campaign. It was worth noting that the $PM_{2.5}$ species and OA composition were substantially different in the polluted period (PP) (BC+NR-$PM_{2.5}$ > 75 μg m^{-3}) and clean period (CP) (BC+NR-$PM_{2.5}$ ≤ 75 μg m^{-3}).

During the PP, the mass concentrations of BC+NR-$PM_{2.5}$ and OA were 102.3 ± 26.9 and 57.4 ± 22.5 μg m^{-3}, 2.5 and 3.1 times that during CP, respectively. Compared with other species, a significantly higher contribution of OA was observed during PP (56.6%) than CP (46.6%) (Student's t-test, $p < 0.001$) (Fig. 2). Here, five OA factors were identified by the PMF-ME2 model with detailed information in SI Text S1, and

https://doi.org/10.5194/egusphere-2025-101
Preprint. Discussion started: 11 April 2025

the mass spectrum of these factors was shown in Fig. S3. Moreover, BBOA showed significant correlations with $C_2H_4O_2^+$ and m/z 73 (r^2 = 0.85, 0.80, p < 0.001); CCOA was strongly correlated with Chl and m/z 115 (r^2 = 0.56, 0.48, p < 0.001); HOA was correlated with NO_2 and m/z 41 (r^2 = 0.47, 0.59, p < 0.001); OOA and aqSOA were significantly correlated with NO_3, NH_4 (r^2 = 0.77, 0.75, p < 0.001) and SO_4, ALWC (r^2 = 0.67, 0.85, p < 0.001), respectively (Fig. S4). These results highlighted the result of five OA factors was reasonable.

It should be noted that the contributions of BBOA and aqSOA to OA increased from CP (31.7% and 12.6%) to PP (38.6% and 14.1%), respectively. Additionally, significantly higher RH and ALWC were observed during PP (58.5 ± 12.4% and 69.4 ± 30.3 μg m^{-3}) than CP (49.8 ± 8.9% and 37.1 ± 20.8 μg m^{-3}) (p < 0.001), but not temperature (p > 0.1). The wind was 0.32 ± 0.18 m s^{-1} during CP, 1.3 times that during PP. These results indicated that the atmosphere was in a stagnant state with relatively high RH and ALWC during PP, which might lead to the largely different sources and chemical processing of OA during CP and PP. As shown in Fig. 2, the obvious diurnal variation of OA concentration with one peak (82.7 μg m^{-3}) appeared at 12:00 local time (LT) in the daytime was exhibited during PP, but 21:00 LT at night during CP. Moreover, OA concentration rapidly increased at a rate of 7.8 μg m^{-3} hr^{-1} from 09:00 to 12:00 LT with a significant decrease of NO_3 during PP. Meanwhile, BBOA and aqSOA concentrations showed similar diurnal patterns to OA concentration with high values in the daytime and rapidly increased from 09:00 to 12:00 LT during PP. Previous research indicated that aqSOA spectrum showed higher

https://doi.org/10.5194/egusphere-2025-101
Preprint. Discussion started: 11 April 2025

m/z 29 (CHO^+) than other OA factors (Gilardoni et al., 2016; Meng et al., 2020; Wang et al., 2021). During PP, the peaks of $C_2H_4O_2^+$ and m/z 29 concentrations, tracer ion fragments of BBOA and aqSOA, were observed at 12:00 LT (1.2 μg m^{-3}) and 13:00 LT (4.3 μg m^{-3}), respectively. Additionally, the correlation between ALWC and aqSOA concentration ($r^2 = 0.86$, $p < 0.001$) was stronger than BBOA concentration ($r^2 = 0.58$, $p < 0.001$), and both ALWC and aqSOA concentration peaks were observed at 13:00 LT, earlier than BBOA concentration peak (12:00 LT), supporting that ALWC might play a significant role in the chemical processing of BBOA and aqSOA during PP.

In summary, these results suggested that OA was the dominant component of $PM_{2.5}$, especially during PP in SCB. During PP, BBOA and aqSOA played important roles in increasing OA concentration in the daytime. Additionally, considerable aqSOA could be formed from BBOA via aqueous-phase reactions under high ALWC in the daytime during PP, which might be related to the frequent fog events and BBOA emissions in the harvest season − autumn − in SCB (Bao et al., 2023; Chen et al., 2017; Chen et al., 2019; Tao et al., 2014). To further explore aqSOA formed from BBOA via the aqueous-phase reactions, the next section would discuss the field observation of aqSOA from biomass-burning emissions.

https://doi.org/10.5194/egusphere-2025-101
Preprint. Discussion started: 11 April 2025

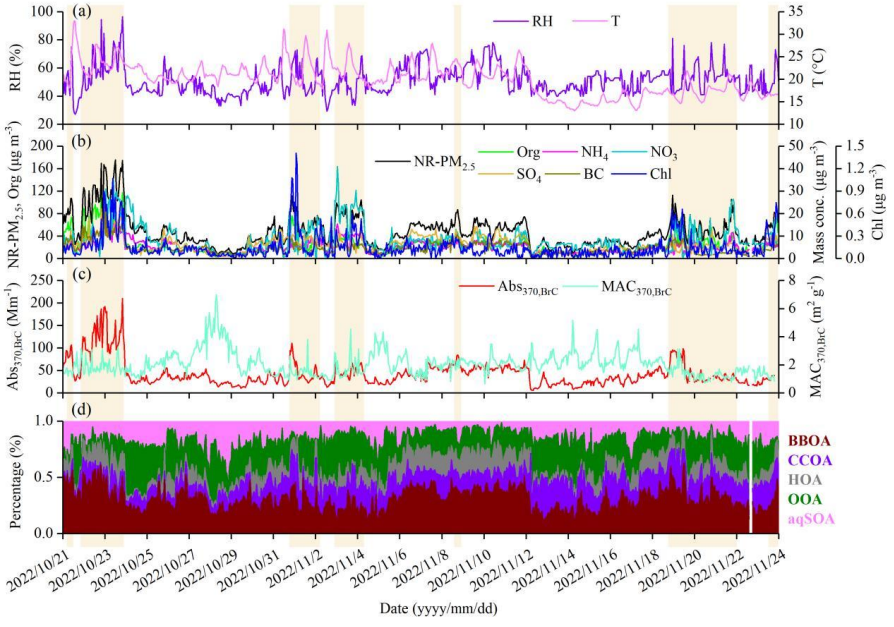

Figure 1. Time series of **(a)** RH and T, **(b)** NR-$PM_{2.5}$ species measured by ToF-ACSM and BC, **(c)** $Abs_{370,BrC}$ and $MAC_{370,BrC}$, and **(d)** mass fraction of OA factors during the campaign. The pollution period (BC+NR-$PM_{2.5}$ > 75 μg m^{-3}) is highlighted by the shaded areas.

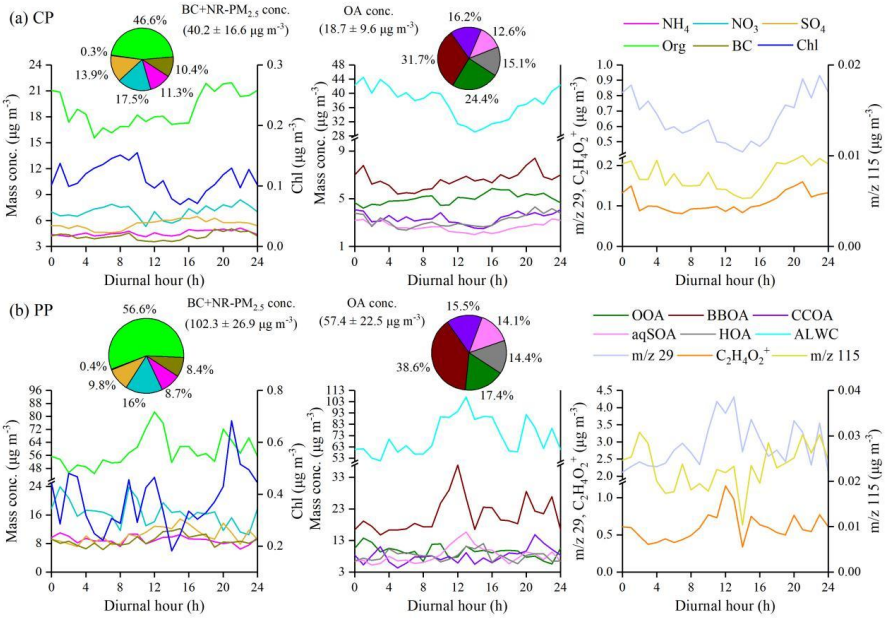

https://doi.org/10.5194/egusphere-2025-101
Preprint. Discussion started: 11 April 2025

Figure 2. Diurnal variations of $PM_{2.5}$ species, BC, OA factors, m/z 29, m/z 115, and $C_2H_4O_2^+$ mass concentrations during **(a)** clean period (CP) (BC+NR-$PM_{2.5}$ < 75 μg m^{-3}) and **(b)** polluted period (PP) (BC+NR-$PM_{2.5}$ > 75 μg m^{-3}). The pie charts in the left side of **(a)** and **(b)** show the average mass contributions of different chemical compositions to BC+NR-$PM_{2.5}$ during CP and PP, respectively. Meanwhile, the average mass contributions of OOA, BBOA, CCOA, aqSOA, and HOA in OA are shown in the pie charts in the middle of **(a)** and **(b)**, respectively.

3.2 Biomass-burning emissions as precursors for aqSOA

Fig. 3 showed the relationship between the mass fraction (%) of aqSOA in total $PM_{2.5}$ and ALWC during the campaign. There was a strong correlation with increasing the contribution of aqSOA at the high f_{29} values (normalized mass spectrum signal at m/z 29) (r^2 = 0.64, p < 0.001). It was important to note that the aqSOA factor showed significantly higher f_{29} and f_{60} values (normalized mass spectrum signal at m/z 60) (0.167 and 0.015) and lower f_{44} value (normalized mass spectrum signal at m/z 44) (0.097) than the OOA factor (0.017, 0.002, and 0.181), respectively (Fig. S3). Moreover, both aqSOA concentrations and f_{29} were well correlated with ALWC (r^2 = 0.85, 0.73, p < 0.001), and the BBOA factor was located in a similar region with aqSOA factor. These results were similar to aqSOA observed in Italy and Beijing (Gilardoni et al., 2016; Zhao et al., 2019), indicating that considerable aqSOA could be formed from biomass-burning OA via aqueous-phase reactions in SCB. Additionally, a strong anticorrelation between the mass fraction of fossil-fuel related OA components (sum of CCOA, HOA and OOA) and ALWC at the high f_{29} values

https://doi.org/10.5194/egusphere-2025-101
Preprint. Discussion started: 11 April 2025

was also observed (r^2 = 0.48, p < 0.001), indicating that aqSOA might also be production by aqueous-phase reactions of fossil-fuel related OA components, consistent with previous research (Wang et al., 2021).

Fig. 4 showed the relationships between ALWC and OA factors or f_{29} during the campaign. Five OA factors mass concentrations increased with the increase of ALWC. However, compared with other OA factors, aqSOA and BBOA significantly increased from 1.1 and 4.9 μg m^{-3} to 5.2 and 10.8 μg m^{-3} when 20 μg m^{-3} < ALWC < 60 μg m^{-3}, respectively. It should be noted that only aqSOA concentrations were even enhancement under high ALWC conditions (> 100 μg m^{-3}), which might be related to more water-soluble organic species (i.e., glyoxal and methylglyoxal) were formed and further formed aqSOA via aqueous-phase reactions in aerosol liquid water (Carlton et al., 2007; Ervens et al., 2011; Tan et al., 2012). Based on the direct observation of aqSOA, Gilardoni et al. (2016) also found that aqSOA such as guaiacol dimer ($C_{14}H_{14}O_4^+$) could be formed from aged biomass-burning emissions at both in fog water and in wet aerosol, especially under high ALWC conditions. As shown in Fig. 4b, the mass fraction of aqSOA showed significant enhancement from less than 5% at ALWC < 20 μg m^{-3} to 17−22% at ALWC > 60 μg m^{-3} with a corresponding decrease in OOA, although POA and SOA contributions were fairly constant across different ALWC levels (58−68% and 32−42%). This result suggested a more intensive formation of aqSOA than OOA via aqueous-phase reactions, although aqSOA might be also formed from OOA, consistent with the recent research in northwest China (Zhao et al., 2019; Zhong et al., 2021). Additionally, the increasing f_{29} (CHO^+) from

https://doi.org/10.5194/egusphere-2025-101
Preprint. Discussion started: 11 April 2025

316 0.010 to 0.227 as a function of ALWC was observed during the campaign (Fig. 4b).
317 The values of f_{29} significantly increased from 0.055 to 0.210 when ALWC increased
318 from 60 μg m^{-3} to 100 μg m^{-3} ($p < 0.001$), consistent with OA mass concentrations
319 (13.2−109.1 μg m^{-3}) during the campaign (Fig. 4b). According to the laboratory
320 analysis of organic standards, previous research found that the spectra of standard
321 organic species without alcohol group showed low f_{29} (< 0.05), while high f_{29} values
322 (0.05–0.15) were found for polyols and species with non-acid OH groups produced
323 from biomass-burning emissions (Canagaratna et al., 2015; Gilardoni et al., 2016;
324 Zhao et al., 2014). This further highlighted the potential formation of organic
325 compounds with hydroxyl groups (i.e., glyoxal and methylglyoxal) under high ALWC
326 conditions. Overall, these results pointed to the fact that the observed aqSOA could be
327 formed from biomass-burning emissions via aqueous-phase reactions, reinforcing the
328 BBOA role in increasing $PM_{2.5}$ mass concentration.

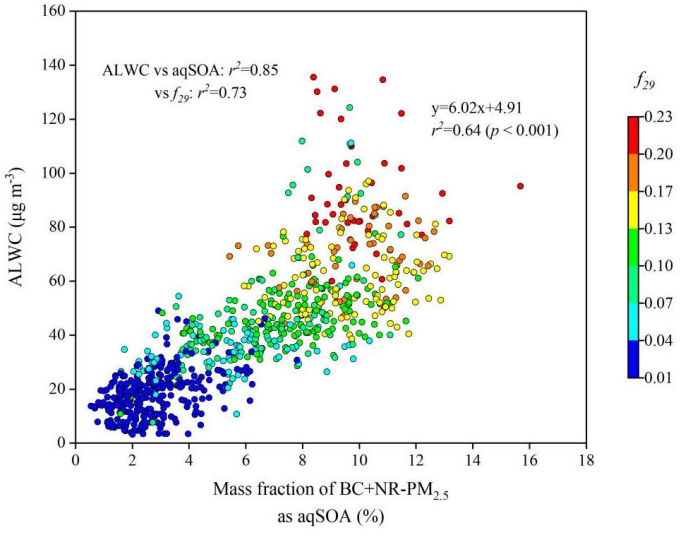

329

330 **Figure 3.** Scatter plot of the mass fraction of aqSOA in BC+NR-$PM_{2.5}$ versus ALWC colored by

https://doi.org/10.5194/egusphere-2025-101
Preprint. Discussion started: 11 April 2025

the f_{29} (normalized mass spectrum signal at m/z 29) during the campaign. f_{29} (mainly CHO^+) is a tracer for alcohol compounds and used to monitor the aqueous-phase oxidation of organic compounds (i.e., glyoxal).

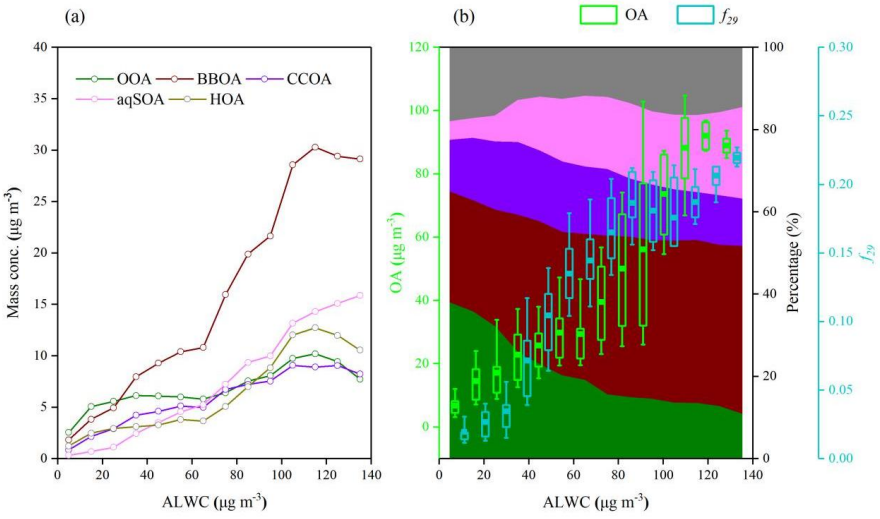

Figure 4. Variations of **(a)** OA factors mass concentrations, and **(b)** OA mass concentrations, f_{29} (a tracer for alcohol compounds), and mass fraction of OA factors as a function of ALWC. The data were grouped into different bins according to a 10 μg m^{-3} increment of ALWC.

To identify the formation of aqSOA and its precursors under different $PM_{2.5}$ pollution levels, the relationship between aqSOA and BBOA or OOA mass concentrations with ion fragments tracers during CP and PP was performed, respectively. As shown in Fig. 5a and c, aqSOA and BBOA concentrations increased with the increase of ALWC in general during CP and PP. However, compared with CP (r^2 = 0.54), the stronger positive correlation between aqSOA and BBOA concentrations was observed during PP (r^2 = 0.64), and so were that between ALWC and aqSOA or BBOA concentrations (r^2 = 0.93, 0.59, respectively). This supported

https://doi.org/10.5194/egusphere-2025-101
Preprint. Discussion started: 11 April 2025

high BBOA concentrations were favorable for aqSOA formation, especially under high ALWC conditions. Fig. 5b and d showed that f_{29} was highly correlated with aqSOA formation during CP and PP. Moreover, it should be noted that a strong anticorrelation between aqSOA and OOA concentrations was observed during PP at ALWC > 80 μg m^{-3} when f_{29} > 0.15 (p < 0.001), but not during CP. These results indicated that considerable aqSOA might be formed from BBOA, which was more intensive than OOA at high ALWC levels during PP.

Previous research demonstrated that f_{44} could be used as a tracer of aged SOA, f_{43} (normalized mass spectrum signal at m/z 43) as a tracer of POA and fresh SOA, and f_{60} as a tracer of BBOA (Cubison et al., 2011; Ng et al., 2010). The triangle plots of f_{44} versus f_{43} and f_{44} versus f_{60} have been widely used to characterize OA evolution, the ratio changes of f_{44} versus f_{43} and f_{44} versus f_{60} as the functions of atmospheric and BBOA aging, respectively (Ortega et al., 2013; Paglione et al., 2020; Xu et al., 2017; Xu et al., 2019). As shown in Fig. 6, the bottom region of the triangle was dominated by BBOA, CCOA, and HOA with low f_{44} (0.040, 0.017, and 0.016, respectively) in this study. However, the f_{44} of SOA factors (i.e., OOA and aqSOA) (0.108 and 0.117) were observably higher than POA factors, showing the freshly oxidized properties of SOA and further aging of OOA might also form aqSOA. Meanwhile, f_{44} of aqSOA was close to that observed in fogs (Gilardoni et al., 2016; Kim et al., 2019), highlighting the presence of aqueous-phase reactions in this study. Fig. 4c showed BBOA and aqSOA with much higher f_{60} values (0.019 and 0.011) than CCOA (0.009) and HOA (0.008). The f_{60} value of OOA was 0.002 lower than the typical background

https://doi.org/10.5194/egusphere-2025-101
Preprint. Discussion started: 11 April 2025

value (0.003) in the atmospheric without biomass burning influence (Cubison et al., 2011). The mass spectrometry feature of aqSOA showed large f_{44} (representation of aged OA) and f_{60} (presence of anhydrosugars) values, laying in a schematic space of aged BBOA based on mass spectrometry features in previous research (Cubison et al., 2011; Ortega et al., 2013). This suggested that BBOA could be the important precursors for aqSOA instead of OOA via aqueous-phase reactions. These results were consistent with previous research and most of the observation data were within the triangle space, indicating that POA factors were freshly emitted and aqSOA were more oxidized from aged BBOA.

During PP, the f_{44} values ranging from 0.022 to 0.140 (0.080 ± 0.035) were significantly higher than that during CP (0.021−0.150, 0.064 ± 0.019) ($p < 0.001$), while the f_{43} value was slightly lower with an average of 0.062 ± 0.027. Compared with CP (0.17 and −0.53), f_{44} showed a more significant increase as the decreasing of f_{43} with higher r^2 value (0.70) and the regression slope of f_{44} versus f_{43} (−1.09) was close to −1 during PP. This indicated that more aged SOA existed in the atmosphere during PP (Fig. 6a and c). It should be noted that the points of f_{44} versus f_{43} were inside the upper boundary of the triangle region, even some were outside the bottom boundary of the triangle region during CP and PP, suggesting that the formation of less oxidized SOA via aqueous-phase reactions instead of photo-chemical reactions (Kim et al., 2019; Zhao et al., 2019). Moreover, these points outside the bottom boundary of the triangle region with higher f_{44} (> 0.05) and lower f_{43} (< 0.06) showed relatively higher ALWC during PP, but not during CP. Overall, these results

https://doi.org/10.5194/egusphere-2025-101
Preprint. Discussion started: 11 April 2025

highlighted the aqSOA with less oxidized formation via aqueous-phase reactions during PP.

Here, the triangle plots of f_{44} versus f_{60} colored by ALWC under different $PM_{2.5}$ pollution levels were analyzed (Fig. 6b and d), when the link between aqSOA and BBOA was further stressed by a schematic representation of aged BBOA. The contribution of f_{60} to different OA factors in this study and previous research was represented in Fig. 6b and d (Bao et al., 2023; Gilardoni et al., 2016; Kim et al., 2019; Ng et al., 2011; Paglione et al., 2020; Xu et al., 2015; Xu et al., 2017; Xu et al., 2019; Zhao et al., 2017; Zhao et al., 2019). The background space (f_{60} < 0.003) without biomass burning influence was also shown by the grey shaded area. All the f_{60} values were higher than 0.003 and most points fell in the triangular region, suggesting the contribution of biomass burning to OA. During PP, The f_{60} values ranging from 0.005 to 0.019 (0.010 ± 0.004) were similar with CP (0.004−0.019, 0.010 ± 0.003), while the mean f_{44} value was significantly higher. Compared with CP, most of the data points with high ALWC fell in the schematic space of aged BBOA, and a stronger negative correlation between f_{44} and f_{60} was observed (r^2 = 0.72, p < 0.001) during PP. Overall, these results pointed to the fact that the observed aqSOA was originated from the aged BBOA via aqueous-phase reactions under high ALWC during PP.

https://doi.org/10.5194/egusphere-2025-101
Preprint. Discussion started: 11 April 2025

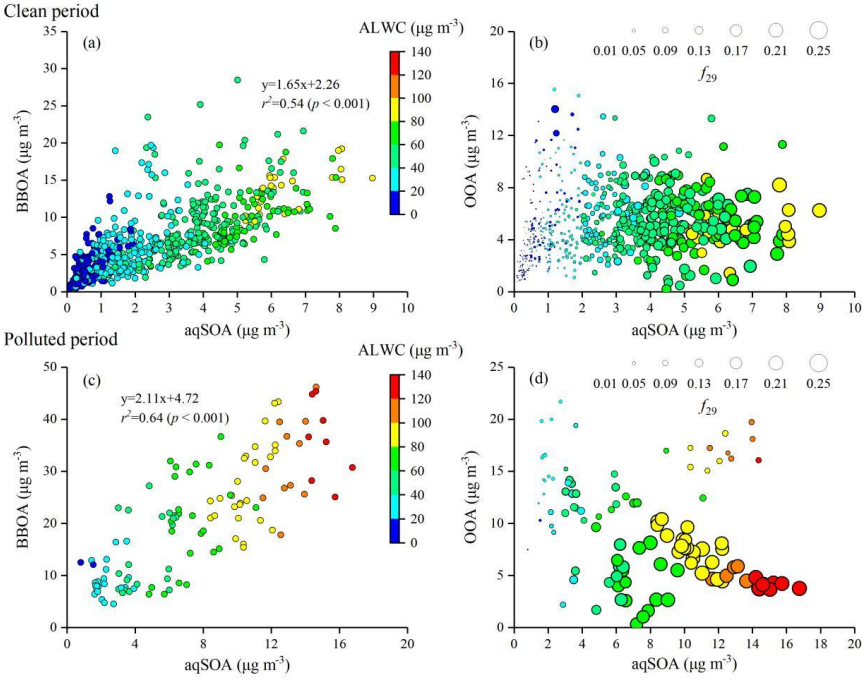

408

409 **Figure 5.** Scatter plots of aqSOA versus **(a, b)** BBOA and **(c, d)** OOA mass concentrations

410 colored by ALWC during clean period and polluted period. The size of the symbols in **(b)** and **(d)**

411 increases with the increase of the f_{29} value, which is a tracer for alcohol compounds.

https://doi.org/10.5194/egusphere-2025-101
Preprint. Discussion started: 11 April 2025

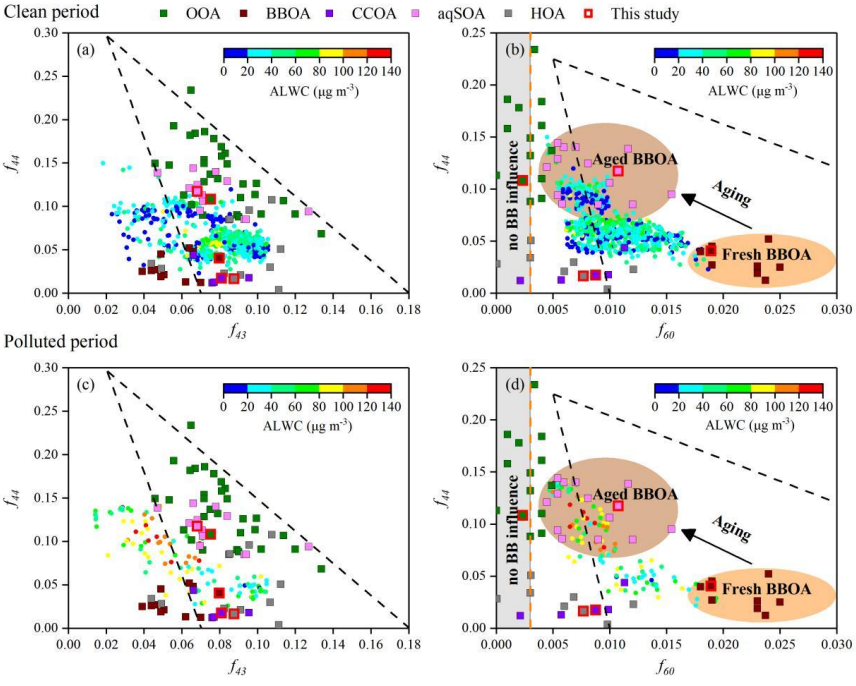

Figure 6. Triangle plots of **(a, c)** f_{44} (normalized mass spectrum signal at m/z 44) versus f_{43} (normalized mass spectrum signal at m/z 43), and **(b, d)** f_{44} versus f_{60} (normalized mass spectrum signal at m/z 60) colored by ALWC during clean period and polluted period. The dashed lines in **(a)** and **(c)** were derived from Ng et al. (2010) and used to follow the aging of OA components in the atmosphere. The background value of secondary aged OA (brown dashed line) and the black dashed lines characterising the aging of BBOA in **(b)** and **(d)** were derived from Cubison et al. (2011). The data points included the measurements in previous studies (Bao et al., 2023; Gilardoni et al., 2016; Kim et al., 2019; Ng et al., 2011; Paglione et al., 2020; Xu et al., 2015; Xu et al., 2017; Xu et al., 2019; Zhao et al., 2017; Zhao et al., 2019). f_{43} (mainly $C_2H_3O^+$) is a tracer for POA and fresh SOA. f_{44} is a proxy of the OA oxygenation degree and used as a tracer for aged SOA. f_{60} is a proxy of anhydrosugars emitted from biomass burning.

https://doi.org/10.5194/egusphere-2025-101
Preprint. Discussion started: 11 April 2025

3.3 Evolution of BrC Absorption

Considerable OA from fresh and aged biomass-burning emissions exhibited absorption properties across UV to Vis range with much higher AAE value than BC (Laskin et al., 2015), might contribute to a net positive radiative forcing. Therefore, the BrC absorption properties and their relationship with five OA factors were analyzed in this study. The values of $Abs_{\lambda,BrC,pri}$ and $Abs_{\lambda,BrC,sec}$ were obtained by MRS method, and the MLR method was used to estimate Abs of five OA factors at each wavelength (SI Text S2,S3). As shown in Fig. S6, the average value of $Abs_{370,BrC}$ was 42.4 ± 28.5 Mm^{-1} (accounting for 49.2% of Abs_{370}), much higher than $Abs_{660,BrC}$ (2.6 ± 1.3 Mm^{-1}, 10.5%), suggesting a high absorption efficiency for BrC in the near-UV wavelength. The $Abs_{\lambda,BrC,pri}$ and $Abs_{\lambda,BrC,sec}$ accounted for 56.8%−72.5% and 27.5%−43.2% of $Abs_{\lambda,BrC}$ from 370 nm to 660 nm respectively, indicating POA was the dominant OA component affecting BrC absorption. However, the contribution of $Abs_{\lambda,BrC,sec}$ to $Abs_{\lambda,BrC}$ increased with wavelength, suggesting the impact on Abs_{BrC} from SOA should not be ignored. Here we showed that aqSOA formation from aged BBOA contributed to the BrC budget and was strong absorption across UV to Vis range.

The data at 370 nm with higher signal-to-noise ratios and Abs_{BrC} contribution was chosen to further analyze the correlations of BrC absorption with various OA components. Compared with CCOA, HOA, and OOA (12.3%, 9.1%, and 11.1%), the Abs at 370 nm calculated for BBOA ($Abs_{370,BBOA}$) and aqSOA ($Abs_{370,aqSOA}$) showed higher contributions (51.9% and 16.4%) to $Abs_{370,BrC}$, consistent with the higher MAC

https://doi.org/10.5194/egusphere-2025-101
Preprint. Discussion started: 11 April 2025

values (Fig. 7). Fig. S8 presented the correlations between $Abs_{370,BrC}$ and the mass concentrations of OOA, BBOA, CCOOA, aqSOA, HOA, and $C_2H_4O_2^+$. $Abs_{370,BrC}$ showed the strongest positive correlations with BBOA and $C_2H_4O_2^+$ (ion fragments tracers of BBOA) concentrations (r^2 = 0.77, p < 0.001), followed by aqSOA concentrations (r^2 = 0.69, p < 0.001). In contrast, the correlations with HOA concentrations (r^2 = 0.36), CCOA (r^2 = 0.25), and OOA (r^2 = 0.09, p > 0.1) were much weaker. The high value and contribution of $Abs_{370,aqSOA}$ and strong positive correlation between $Abs_{370,BrC}$ and aqSOA concentrations could be likely that a portion of aqSOA was formed from aged BBOA via aqueous-phase reactions. Gilardoni et al. (2016) demonstrated that aqSOA formation from aged BBOA via aqueous-phase reactions in the ambient atmosphere contributed to the BrC budget and exhibited slightly higher $AAE_{467–660}$ (AAE of aerosols from 467 nm to 660 nm) values than the fresh and processed biomass-burning emissions in laboratory experiments. The MAC values of the five resolved OA components were shown in Fig. 7. Among these, BBOA showed the highest MAC value (2.37 $m^2\ g^{-1}$), followed by aqSOA (1.23 $m^2\ g^{-1}$) at 370 nm, indicating that the oxidation of BBOA to aqSOA decreased light absorption at short wavelengths. Previous research found that the MAC of BBOA was twice that of SOA associated with water-soluble BrC, such as MAC of BBOA (1.3 ± 0.06 $m^2\ g^{-1}$) was much higher than that for other OA factors at 365 nm (Lorenzo et al., 2017; Washenfelder et al., 2015). However, it should be noted that aqSOA had the lowest $AAE_{370–660,aqSOA}$ value (3.54), while BBOA has the highest $AAE_{370–660,BBOA}$ value (4.93). Moreover, the contribution of aqSOA to Abs_{BrC}

https://doi.org/10.5194/egusphere-2025-101
Preprint. Discussion started: 11 April 2025

increased from 16.4% to 26.7% from 370 to 660 nm, while the contribution from BBOA decreased from 51.9% to 39.1% from 370 to 660 nm. These suggested aqSOA formation from aged BBOA might play an important role in the light absorption of BrC across UV to Vis range.

Fig. S9 showed the ternary contour map to quantify the contribution of BBOA, CCOA, and HOA factors to $Abs_{370,BrC,pri}$, when the strong positive correlation ($p < 0.001$) and high slope of the linear regression (1.80) between BBOA mass concentration and $Abs_{370,BrC,pri}$ were observed. Among these POA factors, the high mass fractions of BBOA to POA were consistent with the high $Abs_{370,BrC,pri}$ values (Fig. S9a). For example, the most data of $Abs_{370,BrC,pri}$ higher than 49.1 Mm^{-1} (90th percentile of $Abs_{370,BrC}$) fell in the region of high BBOA/POA values (> 0.5). Moreover, $Abs_{370,BrC,pri}$ significantly increased with the increases of BBOA and $C_2H_4O_2^+$ mass concentrations with higher r^2 values (0.63 and 0.55) than HOA and CCOA (0.19 and 0.14) (Fig. S9b). These results indicated the major contribution of BBOA to primary BrC light absorption.

During the campaign, the relationship between $Abs_{370,BrC,sec}$ and SOA factors mass concentrations was analyzed to understand the correlation between secondary BrC absorption and its chromophores. As shown in Fig. S10, $Abs_{370,BrC,sec}$ significantly increased with the increase of aqSOA concentrations ($r^2 = 0.44$, $p < 0.001$) and high $Abs_{370,BrC,sec}$ values were consistent with the high ALWC values, but not OOA ($p > 0.1$). Higher slope of the linear regression (3.50) at 370 nm and MAC values across UV to Vis range of aqSOA were also observed than OOA (Fig. 7). To further

https://doi.org/10.5194/egusphere-2025-101
Preprint. Discussion started: 11 April 2025

characterize the evolution of secondary BrC absorption, $Abs_{370,BrC,sec}$ was normalized by ΔCO (the background-corrected CO mixing ratios) to minimize the effect of boundary layer height (Fig. 8) (DeCarlo et al., 2010). Here the background CO value (400 ppb) was defined as the lowest 1.25th percentile of the CO values during the campaign (Kondo et al., 2006). Fig. 8 showed that the values of $Abs_{370,BrC,sec}$/ΔCO increased with the increases of aqSOA and ALWC concentrations especially at night (from 17:00 to 03:00 LT), while $Abs_{370,BrC,pri}$/ΔCO decreased with the increases of BBOA and $C_2H_4O_2^+$ concentrations at night. This suggested considerable secondary BrC chromophores with strong absorption at 370 nm were formed under the high ALWC at night, which might be related to the aqSOA from the aged BBOA via aqueous-phase reactions (Pang et al., 2019; Yu et al., 2016; Zhao et al., 2014). The low values of $Abs_{370,BrC,sec}$/ΔCO at 12:00−14:00 LT should be related to the photolysis and/or photooxidation causing BrC photobleaching (Sareen et al., 2013; Zhao et al., 2015). Overall, we suggested that aqSOA formed from biomass-burning emissions might be important for BrC absorption, especially at night.

$AAE_{370–880}$ was another key parameter to characterize the absorption properties of aerosols, its correlations with the mass fraction of aqSOA (f_{aqSOA}) and BBOA (f_{BBOA}) to OA, and BC-to-OA ratios were shown in Fig. 9. During the campaign, the strong positive correlation ($r^2 = 0.49$, $p < 0.001$) between $AAE_{370–880}$ and f_{aqSOA} was observed with $AAE_{370–880}$ values up to 2.65, while $AAE_{370–880}$ values increased with the slight increase of f_{BBOA} in general ($r^2 = 0.21$, $p < 0.001$) (Fig. 9a and c). Previous laboratory research indicated that the biomass-burning emissions influence on the Abs

https://doi.org/10.5194/egusphere-2025-101
Preprint. Discussion started: 11 April 2025

could be reflected in the relationship between AAE and BC-to-OA ratios (Lu et al., 2015; Saleh et al., 2014). Fig. 9b showed this relationship and $AAE_{370–880}$ values were successfully parameterized by BC-to-OA ratios during the campaign (r^2 = 0.51, p < 0.001). The parameterized curve (black curve) and these data points measured in this study were similar to those reported in the previous laboratory research on biomass-burning emissions using the wavelength from 370 nm to 950 nm (red curve) (Lu et al., 2015). Here, 950 nm and 880 nm were used as the highest wavelength respectively, and similar values were found between $AAE_{370–950}$ and $AAE_{370–880}$ (within 10.0%). It should be noted that the data points of high $AAE_{370–880}$ were consistent with the low BC-to-OA ratios and large f_{aqSOA} values in general. Moreover, the average value of $AAE_{370–880}$ observed in this study (1.95) was higher than $AAE_{370–950}$ observed in the laboratory experiments of fresh and photo-chemically aged biomass-burning emissions (i.e., 1.38 and 1.48 for fresh oak and pocosin pine, 1.42 and 1.73 for aged oak and pocosin pine) (Saleh et al., 2013).

Overall, our ambient observations highlighted the importance of aqSOA formation from aged biomass-burning emissions in contributing to the BrC budget and light absorption, reinforcing aqSOA was an important role in the Sichuan Basin and should be accounted in the air quality budget and climate forcing balance.

https://doi.org/10.5194/egusphere-2025-101
Preprint. Discussion started: 11 April 2025

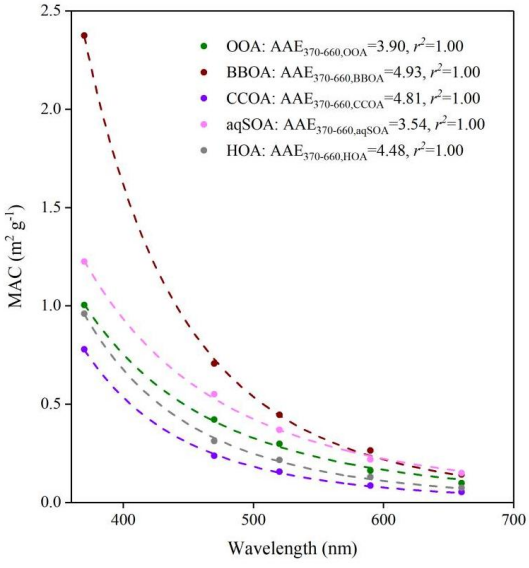

530

531 **Figure 7.** MAC of different OA factors as a function of wavelength from 370 to 660 nm.

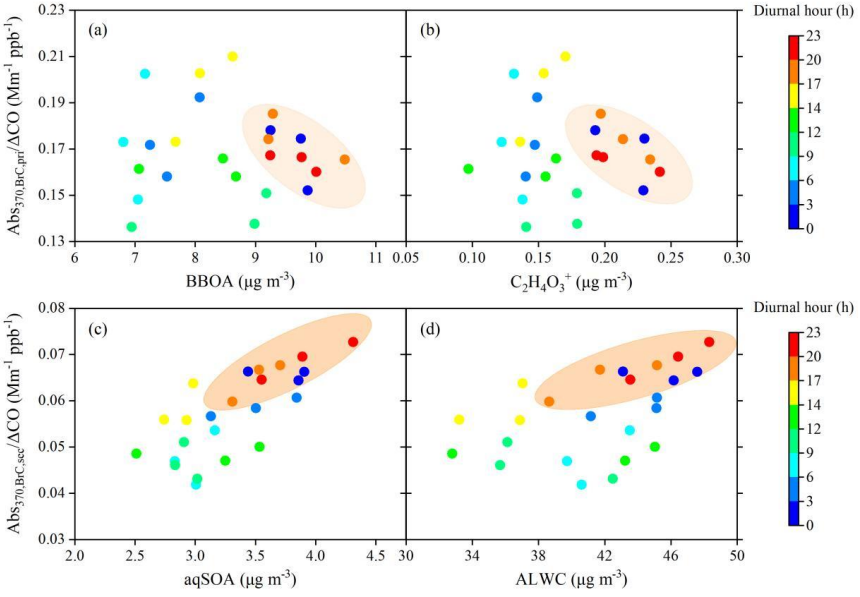

532

533 **Figure 8.** Scatter plots of $Abs_{370,BrC,pri}/\Delta CO$ versus **(a, b)** BBOA and $C_2H_4O_2^+$ mass concentrations

534 and $Abs_{370,BrC,sec}/\Delta CO$ versus **(c, d)** aqSOA and ALWC colored by the local time.

https://doi.org/10.5194/egusphere-2025-101
Preprint. Discussion started: 11 April 2025

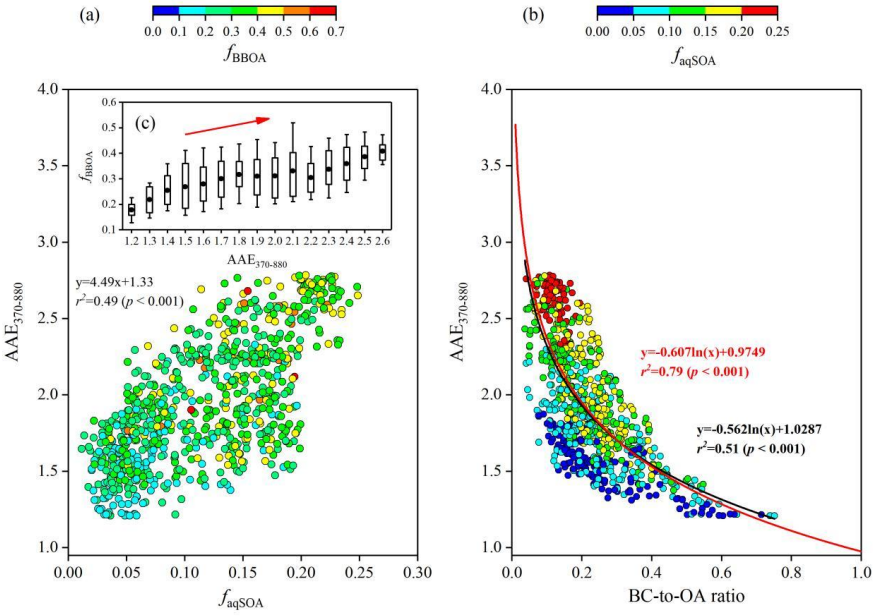

Figure 9. Relationship between **(a)** $AAE_{370–880}$ and the mass fraction of aqSOA (f_{aqSOA} = aqSOA/OA) colored by the mass fraction of BBOA (f_{BBOA} = BBOA/OA), and **(b)** BC-to-OA ratios colored by f_{aqSOA}. **(c)** Variations of f_{BBOA} as a function of $AAE_{370–880}$. The red curve in **(b)** was the best fit curve to data taken from Lu et al. (2015) and described the Abs of fresh and aged BBOA.

4 Implications

Organic aerosol (OA) was the dominant component of atmospheric aerosol with significantly implications for air quality and climate forcing. Field observations indicated that secondary organic aerosol (SOA) accounted for most of OA worldwide and aqueous-phase oxidation was an important pathway for the SOA formation. An increasing laboratory research demonstrated that the aqueous secondary organic aerosol (aqSOA) formed from biomass-burning emissions via aqueous-phase

https://doi.org/10.5194/egusphere-2025-101
Preprint. Discussion started: 11 April 2025

reactions could lead to positive radiative forcing and influence atmospheric photochemistry indirectly (Drozd and McNeill, 2014; Herrmann et al., 2015; Kampf et al., 2012; Nozière and Esteve, 2007; Ye et al., 2019). Our results revealed the aqSOA formation and brownness from aged BBOA via aqueous-phase reactions by the direct ambient observation and highlighted the importance of aqSOA on air quality and climate. The aqSOA formation from aged BBOA contributed to the brown carbon (BrC) budget and showed stronger absorption across ultraviolet to visible range than other OA components. Therefore, the aqueous-phase oxidation of biomass-burning emissions should be taken into account in air quality and climate models for a correct description of the global OA budget and its climate-relevant optical properties.

In this work, the aqSOA formation and absorption properties in the ambient atmosphere were observed directly in the Sichuan Basin, China. The results demonstrated the fact that considerable aqSOA was originated from the aged biomass-burning emissions via aqueous-phase reactions under high ALWC in the ambient atmosphere. Additionally, the less oxidized aqSOA formation via aqueous-phase reactions instead of photo-chemical reactions played a key role in the haze pollution dynamic evolution during the polluted period (Figure 6). This study also indicated that the impact on secondary BrC absorption should not be ignored, although primary BrC dominated the BrC absorption across ultraviolet to visible range. The results of this study highlighted the importance of aqSOA formation from aged biomass-burning emissions in contributing to the BrC budget and absorption,

https://doi.org/10.5194/egusphere-2025-101
Preprint. Discussion started: 11 April 2025

especially at night. Figure 9 further showed that the similarity between ambient data and the parameterized curve of $AAE_{370–880}$ versus BC-to-OA ratios was consistent with the laboratory research on biomass-burning emissions. Higher values of $AAE_{370–880}$ and $MAC_{\lambda,aqSOA}$ reinforced the stronger absorption of aqSOA formation from aged biomass-burning emissions via aqueous-phase reactions than photo-chemically reactions.

In conclusion, our ambient observation demonstrated that the formation and brownness of aqSOA from the aged biomass-burning emissions in the Sichuan Basin, China. Brown aqSOA originating from biomass-burning emissions was an important and unaccounted player in air quality budget and climate forcing balance worldwide. This study was helpful in understanding the formation, light properties, and impacts of aqSOA in the ambient atmosphere. Future research should focus on the molecular-level characterization, transportation, and reactivities of gas and particle-phase aqSOA precursors to improve understanding of aqSOA formation processes and absorption properties.

Data availability. The data generated and analysed in this study are available from https://doi.org/10.5281/zenodo.14626304 (Peng et al., 2025).

Author contributions. CZ, CP, YD, and ZL designed the experiments. Data analysis and interpretation were performed by CP, ZT, HT, KZ, ZL, and GS. CP, XY, and MT wrote the paper. ZT, YC, XL, LZ, YC, and YF contributed to the paper with useful

https://doi.org/10.5194/egusphere-2025-101
Preprint. Discussion started: 11 April 2025

scientific discussions or comments.

Competing interests. The authors declare that they have no conflict of interest.

Acknowledgements. This study was supported by the Natural Science Foundation of Chongqing Municipality (No. CSTB2022NSCQ-MSX0504), National Natural Science Foundation of China (No. 42305126), National Key Research and Development Program of China (No. 2023YFC3709301).

https://doi.org/10.5194/egusphere-2025-101
Preprint. Discussion started: 11 April 2025

References

Bao, Z. E., Zhang, X. Y., Li, Q., Zhou, J. W., Shi, G. M., Zhou, L., Yang, F. M., Xie, S. D., Zhang, D., Zhai, C. Z., Li, Z. L., Peng, C., and Chen, Y.: Measurement report: Intensive biomass burning emissions and rapid nitrate formation drive severe haze formation in the Sichuan Basin, China – insights from aerosol mass spectrometry, Atmos. Chem. Phys., 23, 1147−1167, https://doi.org/10.5194/acp-23-1147-2023, 2023.

Canagaratna, M. R., Jayne, J. T., Jimenez, J. L., Allan, J. D., Alfarra, M. R., Zhang, Q., Onasch, T. B., Drewnick, F., Coe, H., Middlebrook, A., Delia, A., Williams, L. R., Trimborn, A. M., Northway, M. J., DeCarlo, P. F., Kolb, C. E., Davidovits, P., and Worsnop, D. R.: Chemical and microphysical characterization of ambient aerosols with the aerodyne aerosol mass spectrometer, Mass Spectrom. Rev., 26, 185−222, https://doi.org/10.1002/mas.20115, 2007.

Canagaratna, M. R., Jimenez, J. L., Kroll, J. H., Chen, Q., Kessler, S. H., Massoli, P., Hildebrandt Ruiz, L., Fortner, E., Williams, L. R., Wilson, K. R., Surratt, J. D., Donahue, N. M., Jayne, J. T., and Worsnop, D. R.: Elemental ratio measurements of organic compounds using aerosol mass spectrometry: characterization, improved calibration, and implications, Atmos. Chem. Phys., 15, 253−272, https://doi.org/10.5194/acp-15-253-2015, 2015.

Canonaco, F., Crippa, M., Slowik, J. G., Baltensperger, U., and Prévôt, A. S. H.: SoFi, an IGOR-based interface for the efficient use of the generalized multilinear engine (ME-2) for the source apportionment: ME-2 application to aerosol mass

https://doi.org/10.5194/egusphere-2025-101
Preprint. Discussion started: 11 April 2025

621 spectrometer data, Atmos. Meas. Tech., 6, 3649−3661,
622 https://doi.org/10.5194/amt-6-3649-2013, 2013.
623 Carlton, A. G., Turpin, B. J., Altieri, K. E., Seitzinger, S., Reff, A., Lim, H. J., and
624 Ervens, B.: Atmospheric oxalic acid and SOA production from glyoxal: results
625 ofaqueous photooxidation experiments, Atmos. Environ., 41, 7588−7602,
626 https://doi.org/10.1016/j.atmosenv.2007.05.035, 2007.
627 Chen, Y., Tian, M., Huang, R. J., Shi, G. M., Wang, H. B., Peng, C., Cao, J. J., Wang,
628 Q. Y., Zhang, S. M., Guo, D. M., Zhang, L. Y., and Yang, F. M.: Characterization of
629 urban amine-containing particles in southwestern China: seasonal variation, source,
630 and processing, Atmos. Chem. Phys., 19, 3245−3255,
631 https://doi.org/10.5194/acp-19-3245-2019, 2019.
632 Chen, Y., Xie, S. D., Luo, B., and Zhai, C. Z.: Particulate pollution in urban
633 Chongqing of southwest China: Historical trends of variation, chemical
634 characteristics and source apportionment, Sci. Total Environ., 584−585, 523−534,
635 https://doi.org/10.1016/j.scitotenv.2017.01.060, 2017.
636 Coen, M. C., Weingartner, E., Apituley, A., Ceburnis, D., Fierz-Schmidhauser, R.,
637 Flentje, H., Henzing, J. S., Jennings, S. G., Moerman, M., Petzold, A., Schmid, O.,
638 and Baltensperger, U.: Minimizing light absorption measurement artifacts of the
639 Aethalometer: Evaluation of five correction algorithms, Atmos. Meas. Tech., 3,
640 457−474, https://doi.org/10.5194/amt-3-457-2010, 2010.
641 Cubison, M. J., Ortega, A. M., Hayes, P. L., Farmer, D. K., Day, D., Lechner, M. J.,
642 Brune, W. H., Apel, E., Diskin, G. S., Fisher, J. A., Fuelberg, H. E., Hecobian, A.,

https://doi.org/10.5194/egusphere-2025-101
Preprint. Discussion started: 11 April 2025

643 Knapp, D. J., Mikoviny, T., Riemer, D., Sachse, G. W., Sessions, W., Weber, R. J.,
644 Weinheimer, A. J., Wisthaler, A., and Jimenez, J. L.: Effects of aging on organic
645 aerosol from open biomass burning smoke in aircraft and laboratory studies, Atmos.
646 Chem. Phys., 11, 12049−12064, https://doi.org/10.5194/acp-11-12049-2011, 2011.
647 DeCarlo, P. F., Ulbrich, I. M., Crounse, J., de Foy, B., Dunlea, E. J., Aiken, A. C.,
648 Knapp, D., Weinheimer, A. J., Campos, T., Wennberg, P. O., and Jimenez, J. L.:
649 Investigation of the Sources and Processing of Organic Aerosol over the Central
650 Mexican Plateau from Aircraft Measurements during MILAGRO, Atmos. Chem.
651 Phys., 10, 5257−5280, https://doi.org/10.5194/acp-10-5257-2010, 2010.
652 Drinovec, L., Močnik, G., Zotter, P., Prévôt, A. S. H., Ruckstuhl, C., Coz, E.,
653 Rupakheti, M., Sciare, J., Müller, T., Wiedensohler, A., and Hansen, A. D. A.: The
654 "dual-spot" Aethalometer: an improved measurement of aerosol black carbon with
655 real-time loading compensation, Atmos. Meas. Tech., 8, 1965−1979,
656 https://doi.org/10.5194/amt-8-1965-2015, 2015.
657 Drozd, G. T. and McNeill, V. F.: Organic matrix effects on the formation of
658 light-absorbing compounds from α-dicarbonyls in aqueous salt solution, Environ.
659 Sci.: Processes Impacts, 16, 741−747, https://doi.org/10.1039/c3em00579h, 2014.
660 Elser, M., Huang, R. J., Wolf, R., Slowik, J. G., Wang, Q. Y., Canonaco, F., Li, G. H.,
661 Bozzetti, C., Daellenbach, K. R., Huang, Y., Zhang, R. J., Li, Z. Q., Cao, J. J.,
662 Baltensperger, U., El-Haddad, I., and Prévôt, A. S. H.: New insights into $PM_{2.5}$
663 chemical composition and sources in two major cities in China during extreme
664 haze events using aerosol mass spectrometry, Atmos. Chem. Phys., 16, 3207−3225,

https://doi.org/10.5194/egusphere-2025-101
Preprint. Discussion started: 11 April 2025

https://doi.org/10.5194/acp-16-3207-2016, 2016.

Ervens, B., Turpin, B. J., and Weber, R. J.: Secondary organic aerosol formation in cloud droplets and aqueous particles (aqSOA): a review of laboratory, field and model studies, Atmos. Chem. Phys., 11, 11069−11102, https://doi.org/10.5194/acp-11-11069-2011, 2011.

Fountoukis, C. and Nenes, A.: ISORROPIA II: a computationally efficient thermodynamic equilibrium model for K^+–Ca^{2+}–Mg^{2+}–NH_4^+–Na^+–SO_4^{2-}–NO_3^-–Cl^-–H_2O aerosols, Atmos. Chem. Phys., 7, 4639−4659, https://doi.org/10.5194/acp-7-4639-2007, 2007.

Fröhlich, R., Cubison, M. J., Slowik, J. G., Bukowiecki, N., Prévôt, A. S. H., Baltensperger, U., Schneider, J., Kimmel, J. R., Gonin, M., Rohner, U., Worsnop, D. R., and Jayne, J. T.: The ToF-ACSM: a portable aerosol chemical speciation monitor with TOFMS detection, Atmos. Meas. Tech., 6, 3225−3241, https://doi.org/10.5194/amt-6-3225-2013, 2013.

Gilardoni, S., Massoli, P., Paglione, M., Giulianelli, L., Carbone, C., Rinaldi, M., Decesari, S., Sandrini, S., Costabile, F., Gobbi, G. P., Pietrogrande, M. C., Visentin, M., Scotto, F., Fuzzi, S., and Facchini, M. C.: Direct observation of aqueous secondary organic aerosol from biomass-burning emissions, Proc. Natl. Acad. Sci. USA, 113, 10013−10018, https://doi.org/10.1073/pnas.1602212113, 2016.

Hennigan, C. J., Izumi, J., Sullivan, A. P., Weber, R. J., and Nenes, A.: A critical evaluation of proxy methods used to estimate the acidity of atmospheric particles, Atmos. Chem. Phys., 15, 2775–2790, https://doi.org/10.5194/acp-15-2775-2015,

https://doi.org/10.5194/egusphere-2025-101
Preprint. Discussion started: 11 April 2025

687 2015.

688 Herrmann, H., Schaefer, T., Tilgner, A., Styler, S. A., Weller, C., Teich, M., and Otto,
689 T.: Tropospheric Aqueous-Phase Chemistry: Kinetics, Mechanisms, and Its
690 Coupling to a Changing Gas Phase, Chem. Rev., 115, 4259−4334,
691 https://doi.org/10.1021/cr500447k, 2015.

692 Huang, R. J., Zhang, Y. L., Bozzetti, C., Ho, K. F., Cao, J. J., Han, Y. M., Daellenbach,
693 K. R., Slowik, J. G., Platt, S. M., Canonaco, F., Zotter, P., Wolf, R., Pieber, S. M.,
694 Bruns, E. A., Crippa, M., Ciarelli, G., Piazzalunga, A., Schwikowski, M.,
695 Abbaszade, G., Schnelle-Kreis, J., Zimmermann, R., An, Z. S., Szidat, S.,
696 Baltensperger, U., El Haddad, I., and Prevot, A. S.: High secondary aerosol
697 contribution to particulate pollution during haze events in China, Nature, 514,
698 218−222, https://doi.org/10.1038/nature13774, 2014.

699 Jimenez, J. L., Canagaratna, M. R., Donahue, N. M., Prevot, A. S. H., Zhang, Q.,
700 Kroll, J. H., DeCarlo, P. F., Allan, J. D., Coe, H., Ng, N. L., Aiken, A. C., Docherty,
701 K. S., Ulbrich, I. M., Grieshop, A. P., Robinson, A. L., Duplissy, J., Smith, J. D.,
702 Wilson, K. R., Lanz, V. A., Hueglin, C., Sun, Y. L., Tian, J., Laaksonen, A.,
703 Raatikainen, T., Rautiainen, J., Vaattovaara, P., Ehn, M., Kulmala, M., Tomlinson, J.
704 M., Collins, D. R., Cubison, M. J., Dunlea, J., Huffman, J. A., Onasch, T. B.,
705 Alfarra, M. R., Williams, P. I., Bower, K., Kondo, Y., Schneider, J., Drewnick, F.,
706 Borrmann, S., Weimer, S., Demerjian, K., Salcedo, D., Cottrell, L., Griffin, R.,
707 Takami, A., Miyoshi, T., Hatakeyama, S., Shimono, A., Sun, J. Y., Zhang, Y. M.,
708 Dzepina, K., Kimmel, J. R., Sueper, D., Jayne, J. T., Herndon, S. C., Trimborn, A.

https://doi.org/10.5194/egusphere-2025-101
Preprint. Discussion started: 11 April 2025

M., Williams, L. R., Wood, E. C., Middlebrook, A. M., Kolb, C. E., Baltensperger, U., and Worsnop, D. R.: Evolution of Organic Aerosols in the Atmosphere, Science, 326, 1525−1529, https://doi.org/10.1126/science.1180353, 2009.

Kampf, C. J., Jakob, R., and Hoffmann, T.: Identification and characterization of aging products in the glyoxal/ammonium sulfate system – implications for light-absorbing material in atmospheric aerosols, Atmos. Chem. Phys., 12, 6323−6333, https://doi.org/10.5194/acp-12-6323-2012, 2012.

Kim, H., Collier, S., Ge, X. L., Xu, J. Z., Sun, Y. L., Jiang, W. Q., Wang, Y. L., Herckes, P., and Zhang, Q.: Chemical processing of water-soluble species and formation of secondary organic aerosol in fogs, Atmos. Environ., 200, 158−166, https://doi.org/10.1016/j.atmosenv.2018.11.062, 2019.

Kirchstetter, T. W. and Novakov T.: Evidence that the spectral dependence of light absorption by aerosols is affected by organic carbon, J. Geophys. Res., 109, D21208, https://doi.org/10.1029/2004JD004999, 2004.

Kondo, Y., Komazaki, Y., Miyazaki, Y., Moteki, N., Takegawa, N., Kodama, D., Deguchi, S., Nogami, M., Fukuda, M., Miyakawa, T., Morino, Y., Koike, M., Sakurai, H., and Ehara, K.: Temporal Variations of Elemental Carbon in Tokyo, J. Geophys. Res., 111, D12205, https://doi.org/10.1029/2005JD006257, 2006.

Kourtchev, I., Giorio, C., Manninen, A., Wilson, E., Mahon, B., Aalto, J., Kajos, M., Venables, D., Ruuskanen, T., Levula, J., Loponen, M., Connors, S., Harris, N., Zhao, D. F., Kiendler-Scharr, A., Mentel, T., Rudich, Y., Hallquist, M., Doussin, J. F., Maenhaut, W., Bäck, J., Petäjä, T., Wenger, J., Kulmala, Ma., and Kalberer, M.:

https://doi.org/10.5194/egusphere-2025-101
Preprint. Discussion started: 11 April 2025

Enhanced Volatile Organic Compounds emissions and organic aerosol mass increase the oligomer content of atmospheric aerosols, Sci. Rep., 6, 35038, https://doi.org/10.1038/srep35038, 2016.

Kroflic, A., Grilc, M., and Grgic, I.: Unraveling pathways of guaiacol nitration in atmospheric waters: nitrite, a source of reactive nitronium ion in the atmosphere, Environ. Sci. Technol., 49, 9150–9158, https://doi.org/10.1021/acs.est.5b01811, 2015.

Laskin, A., Laskin, J., and Nizkorodov, S. A.: Chemistry of atmospheric brown carbon, Chem. Rev., 115, 4335−4382, https://doi.org/10.1021/cr5006167, 2015.

Li, F. H., Zhou, S. Z., Du, L., Zhao, J., Hang, J., and Wang, X. M.: Aqueous-phase chemistry of atmospheric phenolic compounds: A critical review of laboratory studies, Sci. Total Environ., 856, 158895, https://doi.org/10.1016/j.scitotenv.2022.158895, 2023.

Li, G., Bei, N., Tie, X., and Molina, L. T.: Aerosol effects on the photochemistry in Mexico City during MCMA-2006/MILAGRO campaign, Atmos. Chem. Phys., 11, 5169−5182, https://doi.org/10.5194/acp-11-5169-2011, 2011.

Lim, Y. B., Tan, Y., Perri, M. J., Seitzinger, S. P., and Turpin, B. J.: Aqueous chemistry and its role in secondary organic aerosol (SOA) formation, Atmos. Chem. Phys., 10, 10521−10539, https://doi.org/10.5194/acp-10-10521-2010, 2010.

Lorenzo, R. A. D., Washenfelder, R. A., Attwood, A. R., Guo, H., Xu, L., Ng, N. L., Weber, R. J., Baumann, K., Edgerton, E., and Young, C. J.: Molecular-Size-Separated Brown Carbon Absorption for Biomass-Burning Aerosol

https://doi.org/10.5194/egusphere-2025-101
Preprint. Discussion started: 11 April 2025

753 at Multiple Field Sites, Environ. Sci. Technol., 51, 3128−3137,
754 https://doi.org/10.1021/acs.est.6b06160, 2017.
755 Lu, Z., Streets, D. G., Winijkul, E., Yan, F., Chen, Y., Bond, T. C., Feng, Y., Dubey, M.
756 K., Liu, S., Pinto, J. P., and Carmichael, G. R.: Light absorption properties and
757 radiative effects of primary organic aerosol emissions, Environ. Sci. Technol., 49,
758 4868−4877, https://doi.org/10.1021/acs.est.5b00211, 2015.
759 Matthew, B. M., Middlebrook, A. M., and Onasch, T. B.: Collection Efficiencies in an
760 Aerodyne Aerosol Mass Spectrometer as a Function of Particle Phase for
761 Laboratory Generated Aerosols, Aerosol Sci. Technol., 42, 884−898,
762 https://doi.org/10.1080/02786820802356797, 2008.
763 McNeill, V. F.: Aqueous Organic Chemistry in the Atmosphere: Sources and Chemical
764 Processing of Organic Aerosols, Environ. Sci. Technol., 49, 1237−1244,
765 https://doi.org/10.1021/es5043707, 2015.
766 Meng, J. J., Liu, X. D., Hou, Z. F., Yi, Y. A., Yan, L., Li, Z., Cao, J. J., Li, J. J., and
767 Wang, G. H.: Molecular characteristics and stable carbon isotope compositions of
768 dicarboxylic acids and related compounds in the urban atmosphere of the North
769 China Plain: Implications for aqueous phase formation of SOA during the haze
770 periods, Sci. Total Environ., 705, 135256,
771 https://doi.org/10.1016/j.scitotenv.2019.135256, 2020.
772 Middlebrook, A. M., Bahreini, R., Jimenez, J. L., and Canagaratna, M. R.: Evaluation
773 of Composition-Dependent Collection Efficiencies for the Aerodyne Aerosol Mass
774 Spectrometer using Field Data, Aerosol Sci. Technol., 46, 258−271,

https://doi.org/10.5194/egusphere-2025-101
Preprint. Discussion started: 11 April 2025

https://doi.org/10.1080/02786826.2011.620041, 2012.

Moosmüller, H., Chakrabarty, R. K., and Arnott, W. P.: Aerosol light absorption and its measurement: A review, J. Quant. Spectrosc. Ra., 110, 844−878, https://doi.org/10.1016/j.jqsrt.2009.02.035, 2009.

Ng, N. L., Canagaratna, M. R., Jimenez, J. L., Chhabra, P. S., Seinfeld, J. H., and Worsnop, D. R.: Changes in organic aerosol composition with aging inferred from aerosol mass spectra, Atmos. Chem. Phys., 11, 6465−6474, https://doi.org/10.5194/acp-11-6465-2011, 2011.

Ng, N. L., Canagaratna, M. R., Zhang, Q., Jimenez, J. L., Tian, J., Ulbrich, I. M., Kroll, J. H., Docherty, K. S., Chhabra, P. S., Bahreini, R., Murphy, S. M., Seinfeld, J. H., Hildebrandt, L., Donahue, N. M., DeCarlo, P. F., Lanz, V. A., Prévôt, A. S. H., Dinar, E., Rudich, Y., and Worsnop, D. R.: Organic aerosol components observed in Northern Hemispheric datasets from Aerosol Mass Spectrometry, Atmos. Chem. Phys., 10, 4625−4641, https://doi.org/10.5194/acp-10-4625-2010, 2010.

Ng, N. L., Herndon, S. C., Trimborn, A., Canagaratna, M. R., Croteau, P. L., Onasch, T. B., Sueper, D., Worsnop, D. R., Zhang, Q., Sun, Y. L., and Jayne J. T.: An Aerosol Chemical Speciation Monitor (ACSM) for Routine Monitoring of the Composition and Mass Concentrations of Ambient Aerosol, Aerosol Sci. Technol., 45, 780−794, https://doi.org/10.1080/02786826.2011.560211, 2011.

Nozière, B. and Esteve, W.: Light-absorbing aldol condensation products in acidic aerosols: Spectra, kinetics, and contribution to the absorption index, Atmos. Environ., 2007, 41, 1150−1163, https://doi.org/10.1016/j.atmosenv.2006.10.001,

https://doi.org/10.5194/egusphere-2025-101
Preprint. Discussion started: 11 April 2025

2007.

Ortega, A. M., Ortega, D. A., Cubison, M. J., Brune, W. H., Bon, D., Gouw de, J. A., and Jimenez, J. L.: Secondary organic aerosol formation and primary organic aerosol oxidation from biomass-burning smoke in a flow reactor during FLAME-3, Atmos. Chem. Phys., 13, 11551−11571, https://doi.org/10.5194/acp-13-11551-2013, 2013.

Ortiz-Montalvo, D. L., Lim, Y. B., Perri, M. J., Seitzinger, S. P., and Turpin, B. J.: Volatility and Yield of Glycolaldehyde SOA Formed through Aqueous Photochemistry and Droplet Evaporation, Aerosol Sci. Technol., 46, 1002−1014, https://doi.org/10.1080/02786826.2012.686676, 2012.

Paatero, P.: The Multilinear Engine: A Table-Driven, Least Squares Program for Solving Multilinear Problems, Including the n-Way Parallel Factor Analysis Model, J. Comput. Graph. Stat., 8, 854−888, https://doi.org/10.1080/10618600.1999.10474853, 1999.

Paatero, P. and Tapper, U.: Positive matrix factorization: A non-negative factor model with optimal utilization of error estimates of data values, Environmetrics, 5, 111−126, https://doi.org/10.1002/env.3170050203, 1994.

Paglione, M., Gilardoni, S., Rinaldi, M., Decesari, S., Zanca, N., Sandrini, S., Giulianelli, L., Bacco, D., Ferrari, S., Poluzzi, V., Scotto, F., Trentini, A., Poulain, L., Herrmann, H., Wiedensohler, A., Canonaco, F., Prévôt, A. S. H., Massoli, P., Carbone, C., Facchini, M. C., and Fuzzi, S. C.: The impact of biomass burning and aqueous-phase processing on air quality: a multi-year source apportionment study

https://doi.org/10.5194/egusphere-2025-101
Preprint. Discussion started: 11 April 2025

in the Po Valley, Italy, Atmos. Chem. Phys., 20, 1233−1254, https://doi.org/10.5194/acp-20-1233-2020, 2020.

Pang, H. W., Zhang, Q., Lu, X. H., Li, K. N., Chen, H., Chen, J. M., Yang, X., Ma, Y. G., Ma, J. L., and Huang, C.: Nitrite-Mediated Photooxidation of Vanillin in the Atmospheric Aqueous Phase, Environ. Sci. Technol., 53, 14253−14263, https://doi.org/10.1021/acs.est.9b03649, 2019.

Powelson, M. H., Espelien, B. M., Hawkins, L. N., Galloway, M. M., and Haan, D. O. D.: Brown Carbon Formation by Aqueous-Phase Carbonyl Compound Reactions with Amines and Ammonium Sulfate, Environ. Sci. Technol., 48, 985−993, https://doi.org/10.1021/es4038325, 2014.

Qin, Y. M., Tan, H. B., Li, Y. J., Li, Z. J., Schurman, M. I., Liu, L., Wu, C., and Chan, C. K.: Chemical characteristics of brown carbon in atmospheric particles at a suburban site near Guangzhou, China, Atmos. Chem. Phys., 18, 16409−16418, https://doi.org/10.5194/acp-18-16409-2018, 2018.

Saleh, R., Hennigan, C. J., McMeeking, G. R., Chuang, W. K., Robinson, E. S., Coe, H., Donahue, N. M., and Robinson, A. L.: Absorptivity of brown carbon in fresh and photo-chemically aged biomass-burning emissions, Atmos. Chem. Phys., 13, 7683−7693, https://doi.org/10.5194/acp-13-7683-2013, 2013.

Saleh, R., Robinson, E. S., Tkacik, D. S., Ahern, A. T., Liu, S., Aiken, A. C., Sullivan, R. C., Presto, A. A., Dubey, M. K., Yokelson, R. J., Donahue, N. M., and Robinson, A. L.: Brownness of organics in aerosols from biomass burning linked to their black carbon content, Nat. Geosci., 7, 647−650, https://doi.org/10.1038/ngeo2220,

https://doi.org/10.5194/egusphere-2025-101
Preprint. Discussion started: 11 April 2025

2014.

Sareen, N., Moussa, S. G., and McNeill, V. F.: Photochemical Aging of Light-Absorbing Secondary Organic Aerosol Material, J. Phys. Chem. A, 117, 2987−2996, https://doi.org/10.1021/jp309413j, 2013.

Sun, Y. L., Zhang, Q., Anastasio, C., and Sun, J.: Insights into secondary organic aerosol formed via aqueous-phase reactions of phenolic compounds based on high resolution mass spectrometry, Atmos. Chem. Phys., 10, 4809−4822, https://doi.org/10.5194/acp-10-4809-2010, 2010.

Tan, Y., Lim, Y. B., Altieri, K. E., Seitzinger, S. P., and Turpin, B. J.: Mechanisms leading to oligomers and SOA through aqueous photooxidation: insights from OH radical oxidation of acetic acid and methylglyoxal, Atmos. Chem. Phys., 12, 801−813, https://doi.org/10.5194/acp-12-801-2012, 2012.

Tao, J., Gao, J., Zhang, L., Zhang, R., Che, H., Zhang, Z., Lin, Z., Jing, J., Cao, J., and Hsu, S. C.: $PM_{2.5}$ pollution in a megacity of southwest China: source apportionment and implication, Atmos. Chem. Phys., c14, 8679−8699, https://doi.org/10.5194/acp-14-8679-2014, 2014.

Tian M., Liu Y., Yang F. M., Zhang L. M., Peng C., Chen Y., Shi G. M., Wang H. B., Luo B., Jiang C. T., Li B., Takeda N., and Koizumi K.: Increasing importance of nitrate formation for heavy aerosol pollution in two megacities in Sichuan Basin, southwest China, Environ. Pollut., 2019, 250, 898−905, https://doi.org/10.1016/j.envpol.2019.04.098, 2019.

Wang, G. H., Zhang, R. Y., Gomez, M. E., Yang, L. X., Zamora, M. L., Hu, M., Lin,

https://doi.org/10.5194/egusphere-2025-101
Preprint. Discussion started: 11 April 2025

Y., Peng, J. F., Guo, S., Meng, J. J., Li, J. J., Cheng, C. L., Hu T. F., Ren, Y. Q., Wang, Y. S., Gao, J., Cao, J. J., An, Z. S., Zhou, W. J., Li, G. H., Wang, J. Y., Tian, P. F., Marrero-Ortiz, W., Secrest, J., Du, Z. F., Zheng, J., Shang, D. J., Zeng, L. M., Shao, M., Wang, W. G., Huang, Y., Wang, Y., Zhu, Y. J., Li, Y. X., Hu, J. X., Pan, B., Cai, L., Cheng, Y. T., Ji, Y. M., Zhang, F., Rosenfeld, D., Liss, P. S., Duce, R. A., Kolb, C. E., and Molina, M. J.: Persistent sulfate formation from London Fog to Chinese haze, Proc. Natl. Acad. Sci. USA, 113, 13630−13635, https://doi.org/10.1073/pnas.1616540113, 2016.

Wang, H. B., Tian, M., Chen, Y., Shi, G. M., Liu, Y., Yang, F. M., Zhang, L. M., Deng, L. Q., Yu, J. Y., Peng, C., and Cao, X. Y.: Seasonal characteristics, formation mechanisms and source origins of $PM_{2.5}$ in two megacities in Sichuan Basin, China, Atmos. Chem. Phys., 18, 865−881, https://doi.org/10.5194/acp-18-865-2018, 2018.

Wang, J. F., Ye, J. H., Zhang, Q., Zhao, J., Wu, Y. Z., Li, J. Y., Liu, D. T., Li, W. J., Zhang, Y. G., Wu, C., Xie, C. H., Qin, Y. M., Lei, Y. L., Huang, X. P., Guo, J. P., Liu, P. F., Fu, P. Q., Li, Y. J., Lee, H. C., Choi, H., Zhang, J., Liao, H., Chen, M. D., Sun, Y. L., Ge, X. L., Martin, S. T., and Jacob, D. J.: Aqueous production of secondary organic aerosol from fossil-fuel emissions in winter Beijing haze, Proc. Natl. Acad. Sci. USA, 118, e2022179118, https://doi.org/10.1073/pnas.2022179118, 2021.

Wang, Q. Y., Ye, J. H., Wang, Y. C., Zhang, T., Ran, W. K., Wu, Y. F., Tian, J., Li, L., Zhou, Y. Q., Ho, H. S. S., Dang, B., Zhang, Q., Zhang, R. J., Chen, Y., Zhu, C. S., and Cao, J. J.: Wintertime Optical Properties of Primary and Secondary Brown

https://doi.org/10.5194/egusphere-2025-101
Preprint. Discussion started: 11 April 2025

Carbon at a Regional Site in the North China Plain, Environ. Sci. Technol., 53, 12389−12397, https://doi.org/10.1021/acs.est.9b03406, 2019.

Washenfelder, R. A., Attwood, A. R., Brock, C. A., Guo, H., Xu, L., Weber, R. J., Ng, N. L., Allen, H. M., Ayres, B. R., Baumann, K., Cohen, R. C., Draper, D. C., Duffey, K. C., Edgerton, E., Fry, J. L., Hu, W. W., Jimenez, J. L., Palm, B. B., Romer, P., Stone, E. A., Wooldridge, P. J., and Brown, S. S.: Biomass burning dominates brown carbon absorption in the rural southeastern United States, Geophys. Res. Lett., 42, 653−664, https://doi.org/10.1002/2014gl062444, 2015.

Wu, C. and Yu, J. Z.: Determination of primary combustion source organic carbon-to-elemental carbon (OC/EC) ratio using ambient OC and EC measurements: Secondary OC-EC correlation minimization method, Atmos. Chem. Phys., 16, 5453−5465, https://doi.org/10.5194/acp-16-5453-2016, 2016.

Wu, H., Peng, C., Zhai, T. Y., Deng, J. C., Lu, P. L., Li, Z. L., Chen, Y., Tian, M., Bao, Z. E., Long, X., Yang, F. M., and Zhai, C. Z.: Characteristics of light absorption and environmental effects of Brown carbon aerosol in Chongqing during summer and winter based on online measurement: Implications of secondary formation, Atmos. Environ., 338, 120843, https://doi.org/10.1016/j.atmosenv.2024.120843, 2024.

Xie, C. H., Xu, W. Q., Wang, J. F., Wang, Q. Q., Liu, D. T., Tang, G. Q., Chen, P., Du, W., Zhao, J., Zhang, Y. J., Zhou, W., Han, T. T., Bian, Q. Y., Li, J., Fu, P. Q., Wang, Z. F., Ge, X. L., Allan, J., Coe, H., and Sun, Y. L.: Vertical characterization of aerosol optical properties and brown carbon in winter in urban Beijing, China,

https://doi.org/10.5194/egusphere-2025-101
Preprint. Discussion started: 11 April 2025

907 Atmos. Chem. Phys., 19, 165−179, https://doi.org/10.5194/acp-19-165-2019, 2019.
908 Xu, B. Q., Zhang, G., Gustafsson, Ö., Kawamura, K., Li, J., Andersson, A., Bikkina,
909 S., Kunwar, B., Pokhrel, A., Zhong, G. C., Zhao, S. Z., Li, J., Huang, C., Cheng, Z.
910 N., Zhu, S. Y., Peng, P. A., and Sheng, G. Y.: Large contribution of fossil-derived
911 components to aqueous secondary organic aerosols in China, Nat. Commun., 13,
912 5115, https://doi.org/10.1038/s41467-022-32863-3, 2022.
913 Xu, W. Q., Han, T. T., Du, W., Wang, Q. Q., Chen, C., Zhao, J., Zhang, Y. J., Li, J., Fu,
914 P. Q., Wang, Z. F., Worsnop, D. R., and Sun, Y. L.: Effects of Aqueous-Phase and
915 Photochemical Processing on Secondary Organic Aerosol Formation and Evolution
916 in Beijing, China, Environ. Sci. Technol., 51, 762−770,
917 https://doi.org/10.1021/acs.est.6b04498, 2017.
918 Xu, W. Q., Sun, Y. L., Chen, C., Du, W., Han, T. T., Wang, Q. Q., Fu, P. Q., Wang, Z.
919 F., Zhao, X. J., Zhou, L. B., Ji, D. S., Wang, P. C., and Worsnop, D. R.: Aerosol
920 composition, oxidation properties, and sources in Beijing: results from the 2014
921 Asia-Pacific Economic Cooperation summit study, Atmos. Chem. Phys., 15,
922 13681−13698, https://doi.org/10.5194/acp-15-13681-2015, 2015.
923 Xu, W. Q., Sun, Y. L., Wang, Q. Q., Zhao, J., Wang, J. F., Ge, X. L., Xie, C. J., Zhou,
924 W., Du, W., Li, J., Fu, P. Q., Wang, Z. F., Worsnop, D. R., and Coe, H.: Changes in
925 Aerosol Chemistry From 2014 to 2016 in Winter in Beijing: Insights From
926 High-Resolution Aerosol Mass Spectrometry, J. Geophys. Res.: Atmos., 124,
927 1132−1147, https://doi.org/10.1029/2018JD029245, 2019.
928 Yang, J. W., Au, W. C., Law, H., Lam, C. H., and Nah, T.: Formation and evolution of

https://doi.org/10.5194/egusphere-2025-101
Preprint. Discussion started: 11 April 2025

brown carbon during aqueous-phase nitrate-mediated photooxidation of guaiacol and 5-nitroguaiacol, Atmos. Environ., 254, 118401, https://doi.org/10.1016/j.atmosenv.2021.118401, 2021.

Yang, F. M., Tan, J., Zhao, Q., Du, Z., He, K. B., Ma, Y. L., Duan, F. K., Chen, G., and Zhao, Q.: Characteristics of $PM_{2.5}$ speciation in representative megacities and across China, Atmos. Chem. Phys., 11, 5207−5219, https://doi.org/10.5194/acp-11-5207-2011, 2011.

Ye, Z. L., Qu, Z. X., Ma, S. S., Luo, S. P., Chen, Y. T., Chen, H., Chen, Y. F., Zhao, Z. Z., Chen, M. D., and Ge, X. L.: A comprehensive investigation of aqueous-phase photochemical oxidation of 4-ethylphenol, Sci. Total Environ., 685, 976−985, https://doi.org/10.1016/j.scitotenv.2019.06.276, 2019.

Yu, L., Smith, J., Laskin, A., George, K. M., Anastasio, C., Laskin, J., Dillner, A. M., and Zhang, Q.: Molecular transformations of phenolic SOA during photochemical aging in the aqueous phase: competition among oligomerization, functionalization, and fragmentation, Atmos. Chem. Phys., 16, 4511−4527, https://doi.org/10.5194/acp-16-4511-2016, 2016.

Zhao, J., Du, W., Zhang, Y. J., Wang, Q. Q., Chen, C., Xu, W. Q., Han, T. T., Wang, Y. Y., Fu, P. Q., Wang, Z. F., Li, Z. Q., and Sun, Y. L.: Insights into aerosol chemistry during the 2015 China Victory Day parade: results from simultaneous measurements at ground level and 260 m in Beijing, Atmos. Chem. Phys., 17, 3215−3232, https://doi.org/10.5194/acp-17-3215-2017, 2017.

Zhao, J., Qiu, Y. M.,Zhou, W., Xu, W. Q., Wang, J. F., Zhang, Y. J., Li, L. J., Xie, C.

https://doi.org/10.5194/egusphere-2025-101
Preprint. Discussion started: 11 April 2025

H., Wang, Q. Q., Du, W., Worsnop, D. R., Canagaratna, M. R., Zhou, L. B., Ge, X. L., Fu, P. Q., Li, J., Wang, Z. F., Donahue, N. M., and Sun, Y. L.: Organic Aerosol Processing During Winter Severe Haze Episodes in Beijing, J. Geophys. Res.: Atmos., 124, 10248−10263, https://doi.org/10.1029/2019JD030832, 2019.

Zhao, R., Lee, A. K. Y., Huang, L., Li, X., Yang, F., and Abbatt, J. P. D.: Photochemical processing of aqueous atmospheric brown carbon, Atmos. Chem. Phys., 15, 6087−6100, https://doi.org/10.5194/acp-15-6087-2015, 2015.

Zhao, R., Mungall, E. L., Lee, A. K. Y., Aljawhary, D., and Abbatt, J. P. D.: Aqueous-phase photooxidation of levoglucosan – a mechanistic study using aerosol time-of-flight chemical ionization mass spectrometry (Aerosol ToF-CIMS), Atmos. Chem. Phys., 14, 9695−9706, https://doi.org/10.5194/acp-14-9695-2014, 2014.

Zhong, H. B., Huang, R. J., Chang, Y. H., Duan, J., Lin, C. S., and Chen, Y.: Enhanced formation of secondary organic aerosol from photochemical oxidation during the COVID-19 lockdown in a background site in Northwest China, Sci. Total Environ., 778, 144947, https://doi.org/10.1016/j.scitotenv.2021.144947, 2021.

Zhu, C. S., Cao, J. J., Hu, T. F., Shen, Z. X., Tie, X. X., Huang, H., Wang, Q. Y., Huang, R. J., Zhao, Z. Z., Mocnik, G., and Hansen, A. D. A.: Spectral dependence of aerosol light absorption at an urban and a remote site over the Tibetan Plateau, Sci. Total Environ., 590−591, 14−21, https://doi.org/10.1016/j.scitotenv.2017.03.057, 2017.